Novel Coupling Mechanism−Based Imaging Approach to Scanning Electrochemical Microscopy for Probing the Electric Field Distribution at the Microchannel End

ARTICLE *in* LANGMUIR · SEPTEMBER 2006

Impact Factor: 4.46 · DOI: 10.1021/la0601049 · Source: PubMed

6 AUTHORS, INCLUDING:

Kang Wang
Nanjing University
54 PUBLICATIONS **1,202** CITATIONS
SEE PROFILE

Ai-Lin Liu
Fujian Medical University
44 PUBLICATIONS **723** CITATIONS
SEE PROFILE

Jing-Juan Xu
Nanjing University
266 PUBLICATIONS **8,824** CITATIONS
SEE PROFILE

Xing-Hua Xia
Nanjing University
224 PUBLICATIONS **8,590** CITATIONS
SEE PROFILE

Novel Coupling Mechanism-Based Imaging Approach to Scanning Electrochemical Microscopy for Probing the Electric Field Distribution at the Microchannel End

Kang Wang, Feng-Yun He, Ai-Lin Liu, Jing-Juan Xu, Hong-Yuan Chen, and Xing-Hua Xia*

Key Laboratory of Analytical Chemistry for Life Science, School of Chemistry and Chemical Engineering, Nanjing University, Nanjing 210093, China

Received January 11, 2006. In Final Form: May 18, 2006

A novel coupling mechanism-based imaging approach to scanning electrochemical microscopy (SECM) was used to image the distribution of electric field at the end channel of a poly(dimethylsiloxane) (PDMS) capillary electrophoresis (CE) microchip in the absence of redox species. The coupling imaging mechanism was systematically investigated and qualitatively illustrated. It was proved that the distribution of solution potentials within the scanning plane caused a different reduction rate of water at the tip electrode, which led to the variation in tip current. Within the scanning plane, the solution potentials measured in the central area of the microchannel were usually higher than those measured outside. The SECM images showed a strong dependence on tip potential, tip-to-channel distance, and separation potential. According to the Tafel equation, SECM images were converted to parameters that directly showed the distribution of solution potential. Change in the solution potential along the central axial line of the microchannel was also continuously sensed by allowing the tip to approach the microchannel in the presence of high voltage. Using dopamine as a model compound, the effect of solution potential on electrochemical detection was estimated by detecting separation parameters.

Introduction

An understanding of the spatial distribution of separation electric field in capillary electrophoresis (CE) and microchip CE is one of the fundamental issues for CE systems integrated with electrochemical detection. Several researchers have described the origin of the coupling between the separation electric field and detection electrode.[1−3] Approaches, including decoupling designs, in-channel detection with an electrically isolated potentiostat, and end-channel detection, have been developed to decouple the separation electric field from the detection electrode.[4−11] Klett and Nyholm measured the spatial potential difference in the CE separation using two gold microband electrodes.[2] Manz and co-workers employed the potential difference between the legs of a microfabricated U-shaped floating platinum electrode to form a CE device with wireless electrochemiluminescence detection.[12] Recently, Forry et al. probed the distribution of the electric field along the microfluidic channels by recording fast-scan cyclic voltammetry (FSCV) of a carbon fiber microelectrode inserted into the exit of the microfluidic channels. They illustrated the observed coupling effect by analyzing the different potentials on both sides of the Helmholtz plane.[13] This pioneer work allowed a clear inspection of the electric field distribution inside a separation channel. For further investigation, mapping the electric field distribution at the end of a microchannel is very helpful in evaluating the effect of the separation electric field on end-channel electrochemical detection. Although spatially resolved studies on the influence of the electrode-to-channel position on electrochemical detection have been reported,[2,3,14] as far as we know, no methods have ever been developed to image the separation electric field at the end of a separation channel.

Scanning electrochemical microscopy (SECM) is a scanning probe microscopy technique that has been used for a wide variety of electrochemical studies.[15−17] In a regular SECM system, the probe microelectrode, called the tip electrode, can be precisely positioned several micrometers away from a substrate under the control of a 3D motorized positioner in the solution containing redox-active species. The tip current (i_T) is a function of the tip−substrate distance (d), thus the tip−substrate distance can be directly determined by recording an approach curve (i_T−d curve). By scanning the SECM tip within the plane paralleling a substrate surface and simultaneously monitoring i_T as a function of the tip location, SECM images reflecting the electrochemical properties of the surface could be obtained.[18,19] SECM has been successfully used to image sample surfaces, monitor molecular flux across membranes, and detect metal corrosion and enzyme reaction process.[20−22] White and co-workers created a membrane

* Corresponding author. E-mail: xhxia@nju.edu.cn.

(1) Lu, W.; Cassidy, R. M. *Anal. Chem.* **1994**, *66*, 200−204.
(2) Klett, O.; Nyholm, L. *Anal. Chem.* **2003**, *75*, 1245−1250.
(3) Klett, O.; Bjorefors, F.; Nyholm, L. *Anal. Chem.* **2001**, *73*, 1909−1915.
(4) Lacher, N. A.; Lunte, S. M.; Martin, R. S. *Anal. Chem.* **2004**, *76*, 2482−2491.
(5) Osbourn, D. M. Lunte, C. E. *Anal. Chem.* **2003**, *75*, 2710−2714.
(6) Martin, R. S.; Ratzlaff, K. L.; Huynh, B. H.; Lunte, S. M. *Anal. Chem.* **2002**, *74*, 1136−1143.
(7) Park, S.; Lunte, S. M.; Lunte, C. E. *Anal. Chem.* **1995**, *67*, 911−918.
(8) Wallenborg, S. R.; Nyholm, L.; Lunte, C. E. *Anal. Chem.* **1999**, *71*, 544−549.
(9) Brazill, S. A.; Kim, P. H.; Kuhr, W. G. *Anal. Chem.* **2001**, *73*, 4882−4890.
(10) Huang, X.; Kok, W. T. *J. Chromatogr., A* **1995**, *716*, 347−353.
(11) Lai, C. C. J.; Chena, C. H.; Ko, F. H. *J. Chromatogr., A* **2004**, *1023*, 143−150.
(12) Arora, A.; Eijkel, J. C. T.; Manz, A.; Morf, W. E. *Anal. Chem.* **2001**, *73*, 3282−3288.
(13) Forry, S. P.; Murray, J. R.; Heien, M. L. A. V.; Locascio, L. E.; Wightman, R. M. *Anal. Chem.* **2004**, *76*, 4945−4950.
(14) Matysik, F. M. *Anal. Chem.* **2000**, *72*, 2581−2586.
(15) Nagy, G.; Nagy, L. *Fresenius J. Anal. Chem.* **2000**, *366*, 735−744.
(16) Ameniya, S.; Ding, Z.; Zhou, J.; Bard, A. J. *J. Electroanal. Chem.* **2000**, *483*, 7−17. Kwak, J.; Bard, A. J. *Anal. Chem.* **1989**, *61*, 1794−1799.
(17) Bard, A. J.; Fan, F. R. F.; Kwak, J.; Lev, O. *Anal. Chem.* **1989**, *61*, 132−138.
(18) Wipf, D. O.; Bard, A. J. *Anal. Chem.* **1982**, *64*, 1362−1367.
(19) Lee, C. M.; Wipf, D. O.; Bard, A. J.; Bartels, K.; Bovik, A. C. *Anal. Chem.* **1991**, *63*, 2442−2447.
(20) Zhao, C. A.; Wittstock, G. *Anal. Chem.* **2004**, *76*, 3145−3154.

10.1021/la0601049 CCC: $33.50
Published on Web 07/08/2006

potential through a porous membrane system and analyzed electroosmotic flow in individual pores.[23,24] The influence of the electric field on the tip current was observed, though this influence was not used to develop an imaging mode to probe the distribution of the electric field. Most recently, Roach et al. imaged the continuous emergence of electroactive species by SECM in a CE system in order to improve electrode alignment.[25] However, because a high detection potential was applied to oxidize electrolytes during scanning, they did not find the effect of the solution potential on the tip current. The obtained SECM images showed the distribution of electrolyte flux but not the distribution of electric field at the end channel.

Herein, we describe a method to image the electric field at the end channel of a microchip CE with the help of SECM. In this method, current for water reduction on the tip electrode was used to map the change in solution potential and the level of coupling between the separation electric field and the detection electrode. Therefore, the redox probe or special electroactive species was not required during SECM imaging. Depending on the applied tip potential, separation potential, and tip-to-channel distance, a tip current as high as several hundred nanoamperes was observed. Using this new imaging mode, the channel end can be distinguished more easily than using the feedback imaging mode.[26] The SECM images shown by current could then be transformed into potential-related parameters according to the Tafel equation. The transferred SECM images displayed a clear distribution of the coupling effect at the end of the microchannel. The change of the true tip potential along the axis of microchannel was also proved by detecting separation parameters in the microchip capillary using dopamine as a model compound. This redox probe-free imaging approach can be used to image the electric field distribution on the filter membrane or cell membranes.

Experimental Section

Reagents. Dopamine hydrochloride was obtained from Sigma. Hexaammineruthenium (III) chloride ($Ru(NH_3)_6Cl_3$) was purchased from Aldrich. Poly(dimethylsiloxane) (PDMS) base and curing agent (Sylgard 184, Dow Corning, Midland, MI) were used as received. All of the other reagents were of analytical grade. Phosphate buffer solution (PBS, 5 mM, pH 7.4) was used as a separation medium of CE. All solutions were prepared with PBS, and the dopamine solution was freshly prepared. Deionized water was used to prepare all of the aqueous solutions (>18.2 MΩ, Purelab Classic Corp.).

Apparatus. The arrangement of the end-channel amperometric detection CE−EC system is schematically shown in Figure 1. This microchip CE−EC system is composed of two independent parts: an SECM system and a microchip electrophoresis system.

A model CHI 900 SECM (CH Instruments, Austin, TX) was used to record SECM images. A three-electrode configuration was used for all amperometric detection with a microdisk Pt tip ($a = 5$ μm; RG = 10, insulated in glass) as the working electrode, a Pt wire as the counter electrode, and Ag/AgCl (in 3 M KCl) as the reference electrode.

A typical cross-type channel of poly(dimethylsiloxane) (PDMS) was fabricated following the process described previously.[27] The resulting effective separation channel was 33 mm in length. Scanning electron microscopy (Hitachi X-650, Japan) measurement showed

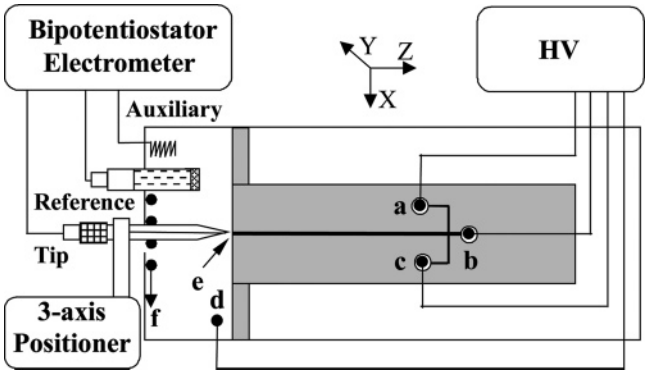

Figure 1. Schematic diagram of the microchip CE−end channel amperometric detection combined with an SECM. (a) Injection (+), (b) separation (+), (c) injection (ground), (d) separation (ground), (e) end channel, and (f) silicone grease. The silicone grease was used to keep the tip movable as well as prevent solution in the detection reservoir from leaking outside the gap between the tip and the reservoir wall.

that the cross section of the channel was 45 μm wide at the top, 65 μm wide at the bottom, and 14 μm in height.[26] Then, the cross sections (end channel) of two chip slabs were carefully adjusted into one plane under an optical microscope (JNOEC JSZ8, China). A homemade voltage power supplier (voltage range: 0 to +5000 V) was used for all of the electrophoresis experiments. For the electrophoresis procedure, the injection was carried out by applying a high voltage (HV) of 1000 V to the sample reservoir for 1 s. Once the sample injection was completed, a separation voltage of 1000 V was applied to the buffer reservoirs with the detection reservoir grounding and the other reservoirs floating. Typically, the separation current was 2.2 ± 0.1 μA.

SECM Tip Positioning and Imaging. Before measurement, the tip electrode approached the cross section of a microchip in 1 mM $Ru(NH_3)_6Cl_3$ solution while the tip was polarized at −0.3 V in the absence of separation HV. The electrode-to-channel distance was calculated according to ref 28. To position the tip electrode at different parts of the channel end, SECM images based on the feedback imaging mode were recorded, and then the tip-to-channel position could be controlled according to the obtained image. A detailed description of this approach has been reported previously.[26] Coupling images were recorded under a separation HV of 1000 V when the whole system was filled with pure running buffer. It is worth noting that coupling imaging can be collected in buffer solution directly after the approaching step. The feedback images are just recorded to compare with the coupling images.

Safety Considerations. The high-voltage power supplier should be handled with extreme care to avoid electrical shock.

Results and Discussion

Imaging Electric Field at the End Channel of the Microchip. Figure 2 shows the SECM images recorded at a tip-to-channel distance of 11 μm within a scanning plane lying parallel to the end channel. The SECM feedback image was first recorded in a solution containing redox reagent (Figure 2a). From Figure 2a, the edge of the trapeziform channel can be easily identified (shown by dashed lines), which falls in line with our previous results.[26] Because the scanning plane was not absolutely parallel to the cross section of the microchip, the currents in upper right part were higher than those in the lower left part. For the relative softness of PDMS, the tiny internal force between two PDMS slabs sometimes slightly distorts the cross section of the microchannel. The SECM image was also recorded at the same location with separation high voltage in the absence of redox species (Figure 2b). The SECM image in Figure 2b shows a

(21) Uitto, O. D.; White, H. S.; Aoki, K. *Anal. Chem.* **2002**, *74*, 4577−4582.
(22) Turyan, I.; Matsue, T.; Mandler, D. *Anal. Chem.* **2000**, *72*, 3431−3435.
(23) Uitto, O. D.; White, H. S. *Anal. Chem.* **2001**, *73*, 533−539.
(24) Bath, B. D.; Lee, R. D.; White, H. S.; Scott, E. R. *Anal. Chem.* **1998**, *70*, 1047−1058.
(25) Roach, D. M.; Hooper, S. E.; Anderson, M. R. *Electroanalysis* **2005**, *17*, 2254−2259.
(26) Wang, K.; Xia, X. H. *J. Chromatogr., A* **2006**, *1110*, 222−226.
(27) He, F. Y.; Liu, A. L.; Xia, X. H. *Anal. Bioanal. Chem.* **2004**, *379*, 1062−1067.
(28) Amphlett, J. L.; Denuault, G. J. *J. Phys. Chem. B* **1998**, *102*, 9946−9951.

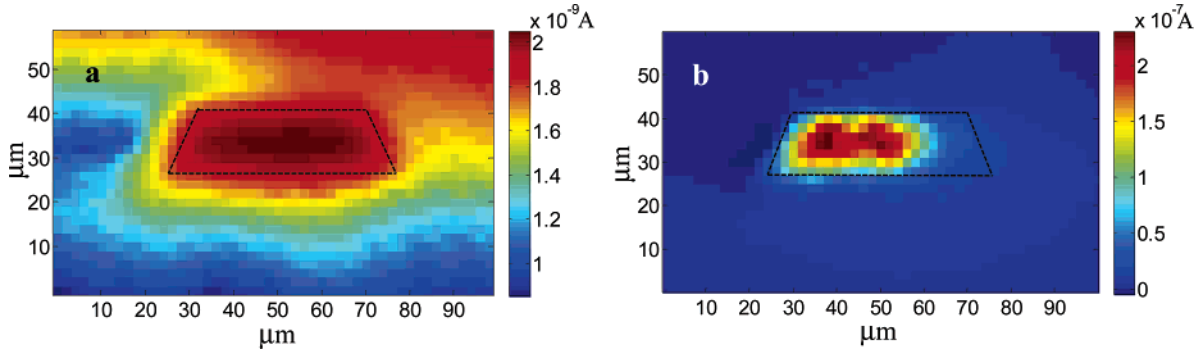

Figure 2. SECM images measured at the end of a PDMS microchannel. Tip potential: −0.3 V, electrode-to-channel distance: 11 μm. (a) SECM image obtained in feedback mode in 1 mM $Ru(NH_3)_6Cl_3$ solution without separation high voltage. (b) SECM image recorded in 5 mM phosphate buffer (pH 7.4) with a separation HV of 1000 V. Dashed lines showed the approximate boundary of the microchannel, which were drawn according to the feedback current in part a.

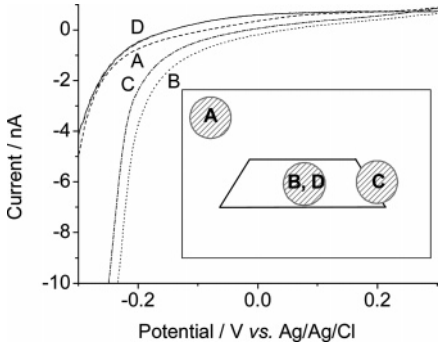

Figure 3. Linear sweep voltammograms of a Pt tip electrode at different tip-to-channel positions. A, B and C were measured with a separation HV of 1000 V, and D was measured without a separation HV. Measured in PBS solution; scan rate: 50 mV/s; detection distance: 11 μm. The inset shows the lateral tip-to-channel position.

trapeziform similar to the microchannel observed in Figure 2a. Although the redox reagent was completely removed from the experimental system before imaging, much higher tip current (ca. 100 times) appeared inside the microchannel. The current gradient also showed an obvious dependence on the channel shape. The imaging mechanism of such a "strange" SECM image was first qualitatively analyzed and then experimentally proved. In Figure 2b, the tip electrode gave a maximum current of 2.32 $\times 10^{-7}$ A. Because no redox species existed in the buffer solution, such a high current could not be caused by the convection of solution or the change in flux at the channel opening. Meanwhile, because the saturation concentration of oxygen in aqueous solution is very low at the experimental temperature (ca. 1×10^{-4} M), the reduction of oxygen dissolved in solution could not give such a high current. As a result, it is reasonable to assign this high current to water reduction at the tip electrode. The fact is that under high tip current, bubbles could be observed in the tip-to-channel gap after a long-time scan, which also suggests that water is reduced at the tip electrode. Considering that oxygen was not removed from the system, the observed high tip current could be caused by the reduction of both oxygen and water. When no separation HV was applied, featureless SECM images were usually obtained (Figure S1). This result indicates that the trapeziform observed in Figure 2b is not related to the flux of buffer or oxygen diffusion at the channel end but to the change in tip potential caused by the HV distribution.

To prove the hypothesis mentioned above, linear sweep voltammorgrams were recorded at different tip-to-channel positions (Figure 3), and the corresponding positions were shown in the inset. When no HV was applied to the microchannel (Figure 3, curve D), the linear sweep voltammogram of the Pt tip showed an increasing reduction current starting at around −0.2 V. At a tip potential of −0.3 V, the tip current was lower than 2 nA. Upon application of a separation HV to the microchannel, a minor positive shift of the measured voltammogram at position A was observed (Figure 3, curve A). This positive shift became obvious when the tip electrode was positioned at the edge (Figure 3, curve C) or in the center of the channel (Figure 3, curve B). Results in Figure 3 are not fully novel because it is well known that solution potentials near the channel end are different from those near the reference electrode.[2,3,12] However, Figure 3 also shows a clear gradient of solution potential in the vicinity of the channel end. From the center (position B) to the edge of the channel (point C) and the spots far away from the channel center (e.g., point A), the solution potential decreases gradually. When a constant potential was applied during SECM imaging (such as −0.3 V), a higher reduction current was obtained at position B because the solution potential increased and consequently the interfacial potential shifted negatively. Though a quantitative determination of the difference in solution potential by voltammograms of the oxygen/water reduction reaction depends on the interfacial state of the Pt electrode, the potential has a significant tendency to shift with detection position.

For a better understanding of the imaging mechanism (Figure 2b), it is important to find out the reason for the change in solution potential at the channel end. Though the *iR* drop in a capillary electrophoresis process dominantly occurs in the separation capillary channel, a minor part of the separation electric field disperses in the detection reservoir because of the finite resistance of the microchannel.[1−3,12,29,30] This dispersing electric field results in a potential gradient in the detection reservoir and changes the solution potential around the detection electrode. Therefore, the solution potential couples with the detection electrode, and its distribution will be of a different coupling level at each individual position. The coupling effect has been illustrated by several researchers.[2,3,12,14] Here, a method similar to Forry's was employed to demonstrate the imaging mechanism.[13] Figure 4 schematically shows the potential drop across the Helmholtz plane, which corresponds to different positions shown in the inset of Figure 3. The real interfacial potentials at positions A, B, and C are defined as E_A, E_B, and E_C, and the solution potentials caused by the applied separation potential are defined as $E_{A,S}$, $E_{B,S}$, and $E_{C,S}$, respectively. In the absence of the separation potential, the interfacial potential is equal to that applied by the potentiostat (E_{app}). Because the voltage power supply provides a positive HV corresponding to the grounding end, the solution potential at the outer Helmholtz plane increases after the separation potential is applied (Figure 1). The solution potential is different at each spot within the scanning plane, which causes a change

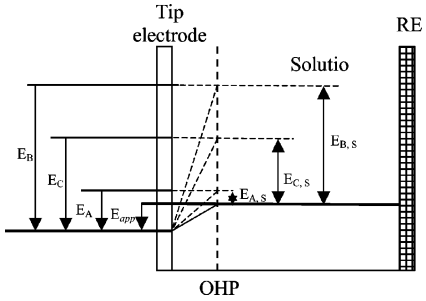

Figure 4. Diagram of interfacial potential at different positions within the scanning plane. In this illustration, distances are not to scale. The potential drop at the reference electrode (RE) has been neglected. OHP: outer Helmholtz plane of the tip electrode. E_A, E_B, and E_C: real interfacial potentials of the tip electrode at corresponding positions in the inset of Figure 3. $E_{A,S}$, $E_{B,S}$, and $E_{C,S}$: solution potentials at the corresponding positions. E_{app}: tip potential given by a potentiostat. Note that when the tip current is low, $E_A = E_{app} + E_{A,S}$, $E_B = E_{app} + E_{B,S}$, and $E_C = E_{app} + E_{C,S}$. When the tip current is high, the real potential applied to the tip electrode (E'_{app}) would be smaller than E_{app} because of the *iR* drop in solution.

in the interfacial potentials of the tip electrode and finally results in a different tip current.

In our case, Figure 2b shows higher tip currents at positions "inside" the microchannel, which indicates that solution potentials at positions "inside" the microchannel within the scanning plane are higher than those at "outside" positions. Because the scanning plane was slightly nonparallel to the cross section of the microchannel in Figure 2a, the highest tip current did not occur exactly in the center of the trapeziform microchannel. Because the tip-to-channel distance in the upper right part of the microchannel was a bit larger than that in the lower left, the tip current decreased gradually in the right half of the microchannel. However, the relatively large size of the insulating glass of the tip electrode (100 μm in diameter) may also cause a distortion of the electric field distribution, leading to the sharp decrease in the tip current at the left edge of the microchannel in Figure 2b. Further research on detecting the electric field distribution with submicrometer-sized tips is ongoing.

Parameters Influencing Coupling Imaging. It can be deduced from Figure 3 that the tip current obtained with the coupling effect is also determined by the tip potentials. At a higher tip potential such as +0.2 V, the change in solution potential (about +0.1 V at position B in Figure 3) could only lead to a tip current change of less than 1 nA. Figure 3 demonstrates that, at higher tip potentials, a decreasing interfacial potential could not significantly enhance the reduction reaction rate at the tip electrode. SECM images measured at different tip potentials are shown in Figure 5. At a potential of 0.5 V (Figure 5a), only very low tip currents were observed, thus the position of mirochannel could not be clearly identified. However, a distinct SECM image could be obtained at a tip potential of −0.2 V (Figure 5b). A series of images were collected with tip potentials ranging from −0.3 to +0.7 V (not shown). In brief, higher tip currents could be observed at lower tip potentials, and lower tip currents or even featureless SECM images appeared at relatively higher tip potentials. This result falls in line with our deduction from Figure 3 and strongly suggests that the SECM images that we obtain in this report are essentially different from those that Roach et al. obtained by measuring the continuous emergence of electroactive species in a CE system.[25] In their experiments, 0.65 V was applied to the detection electrode to oxidize the analytes. At such a tip potential, the coupling-induced decrease in the tip potential had a negligible effect on the tip current. In addition, their carbon-fiber disk electrode has a larger overpotential for the oxygen/water reduction reaction as compared to that of the Pt electrode. Therefore, their SECM images show only the distribution of electrolyte flux.

The tip current in SECM images also depends on the applied separation potential. As shown in Figure 6a−c, at a constant tip potential of 0 V the maximum current of the SECM image increased from 3.85×10^{-9} to 1.24×10^{-8} A as the separation voltage increased from 1200 to 1600 V. This Figure demonstrate that the solution potential around the channel end is a function of the applied separation potential as well. The red region in Figure 6a−c became flattened along with the increase in separation voltage, which might be caused by two factors. First, the tip current was used to reflect the change in solution potential in this work. As indicated in Figure 3, the reduction of water/oxygen starts at the tip potential of 0 V. For an electrochemical reaction whose rate is limited by the surface process, the current and overpotential satisfy the Tafel equation[31]

$$i = a' e^{\eta/b'}$$

or

$$\ln i = a + b\eta$$

where a, b, a', and b' are constants and η denotes the overpotential. With the increase in the separation HV, the solution potential in the central part of the microchannel increases faster than that in the outside regions. Consequently, the absolute tip currents in the central part of the microchannel increased much faster than those measured at other positions. As the colors of the SECM image were ranked by the ratio of the tip current to the highest tip current within the scanning plane, a flattened shape corresponding to the center of microchannel was highlighted. Second, the relatively large tip created a thin layer between the tip and the microchannel. Under lower separation HV (Figure 6a and b), the *iR* drop caused by this thin layer was neglectable. However, at higher separation HV (Figure 6c), this *iR* drop became another source that affected the distribution of the electric field at the end channel. To avoid such a distortion caused by the *iR* drop, either a smaller tip or a lower electric field is required.

In Figure 6, images d, e, and f were translated from images a, b, and c, respectively, by replotting the SECM images with ln *i*. At the tip potentials used in this research, the reduction of oxygen/water or the oxidation of water approximately satisfied the Tafel equation (Figure 3). The SECM images shown by ln *i* roughly represent the distributing tendency of solution potentials within the scanning plane. Figure 6d−f shows that within the scanning plane the solution potentials in the central part of the microchannel were higher than those outside. Though the electric field was distorted along with the increase in separation HV, the highest solution potential stays in the central part of the microchannel. The highest value of ln *i* increased from image d to f, which directly showed the dependence of solution potential on the separation HV.

SECM images were also recorded at different tip-to-channel distances in the presence of separation HV. As shown in Figure 7, the tip current and ln *i* in the "center" of the channel measured at a tip-to-channel distance of 12 μm (Figure 4a and c) were larger than those at a distance of 17 μm (Figure 7b and d), demonstrating that the solution potential increased along the central axial line of the microchannel. In Figure 7c, ln *i* ranged

(29) Hebert, N. E.; Kuhr, W. G.; Brazill, S. A. *Anal. Chem.* **2003**, *75*, 3301−3307.
(30) Wallingford, R. A.; Ewing, A. G. *Anal. Chem.* **1987**, *59*, 1762−1766.
(31) Bard, A. J.; Faulker, L. R. *Electrochemical Methods: Fundamentals and Applications*; Wiley: New York, 1980; pp 91−92.

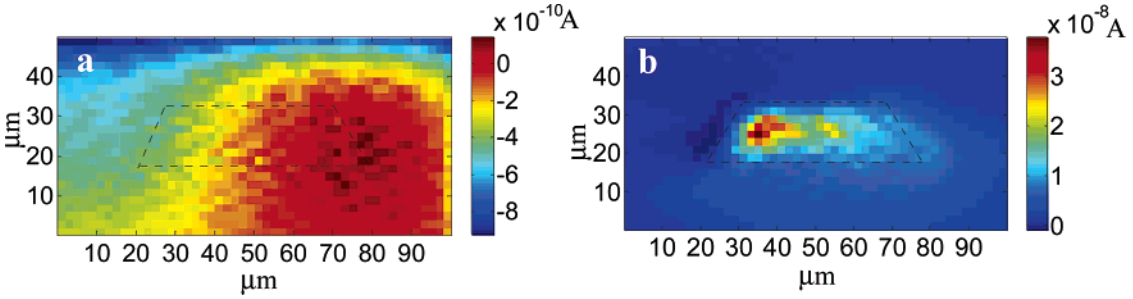

Figure 5. SECM images measured at different tip potentials at a tip-to-channel distance of 11 μm and a separation potential of 1000 V. (a) Tip potential of 0.5 V; (b) tip potential of −0.2 V. Other conditions are the same as in Figure 2. It should be noted that the current scales are (a) 10^{-10} A and (b) 10^{-8} A.

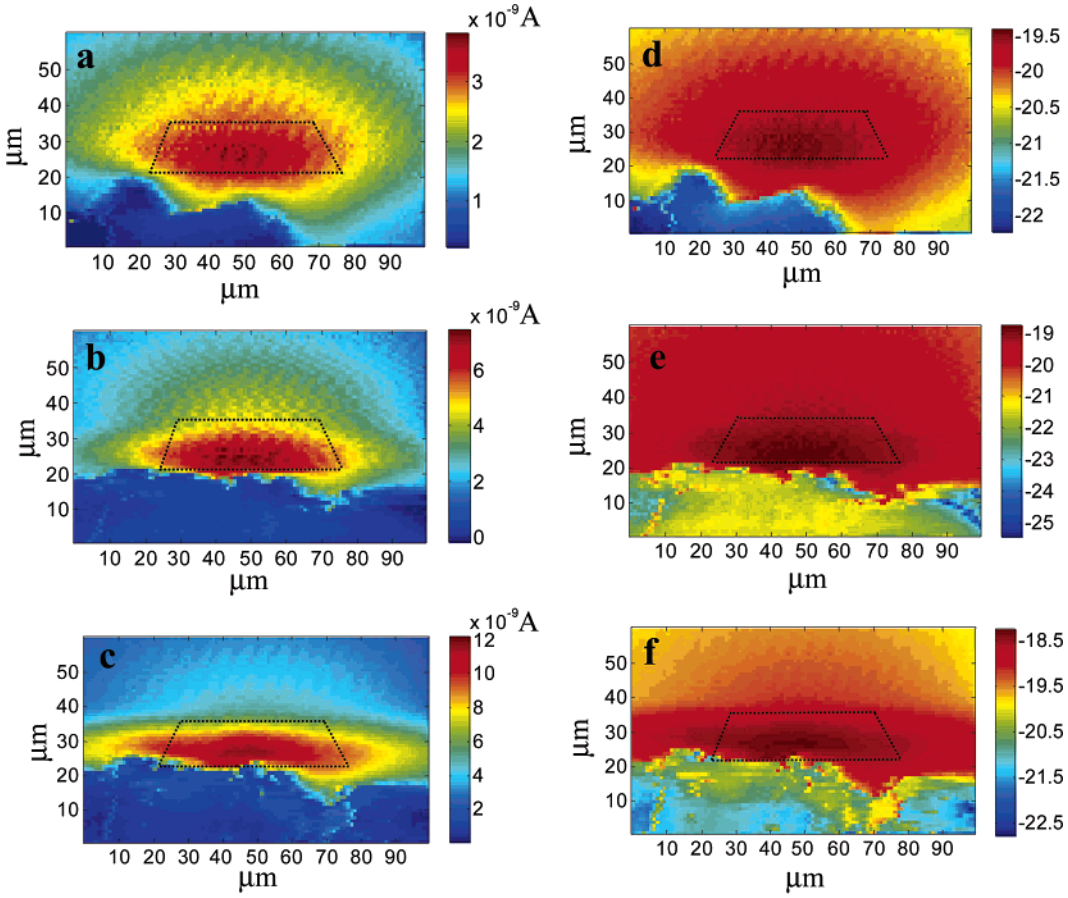

Figure 6. SECM images obtained at different separation potentials at a tip potential of 0 V and an electrode-to-channel distance of 11 μm. Separation HV: (a, d) 1200 V; (b, e) 1400 V; (c, f) 1600 V. Images d, e, and f were translated from images a, b, and c, respectively, and are shown in ln *i*. Other conditions were the same as in Figure 2. It should be noted that the scales of images d, e, and f are negative.

from −20 to about −15.6, and it was much larger than that shown in Figure 7d (−21.2 to about −17.9). The above results show that the variation in solution potential within the scanning plane near the end channel is more significant than that far from the end channel. Therefore, at a short tip-to-channel distance, the solution potential increases, and the coupling effect shows a stronger dependence on the tip-to-channel position. This result also shows the importance of tip-to-channel alignment in the CE system with electrochemical detection, which has been described by many researchers.[14,32−34] When the tip is not positioned in the center of the microchannel, the coupling effect between the tip and the separation electric field will be different. Such a difference may lead to inferior reproducibility among batches of measurements.

Continuously Sensing Solution Potential along the Central Axial Line of a Microchannel. On the basis of the coupling images, the tip electrode can be easily aligned with the center of the microchannel. Solution potential along the central axial line of the microchannel can then be sensed continually by recording the tip approach curve under separation HV. Figure 8 shows the approach curve recorded with a tip potential of 1 V and a separation HV of 1000 V. The current was converted to ln *i* to show the change in solution potential during approach. The current approach curve (i−d) was shown in the inset (Figure 8, inset, open circles). The tip-to-channel distance was obtained by first recording an approach curve on the cross section of the microchip with the SECM feedback mode (Figure 8, open triangles). Then the approach curve was compared with the

(32) Bao, N. Xu, J. J. Dou, Y. H.; Cai, Y.; Chen, H. Y.; Xia, X. H. *J. Chromatogr., A* **2004**, *1041*, 245−248.
(33) Matysik, F. M. *J. Chromatogr., A* **1996**, *742*, 229−234.
(34) Rossier, J. S.; Ferrigno, R.; Girault, H. H. *J. Electroanal. Chem.* **2000**, *492*, 15−22.

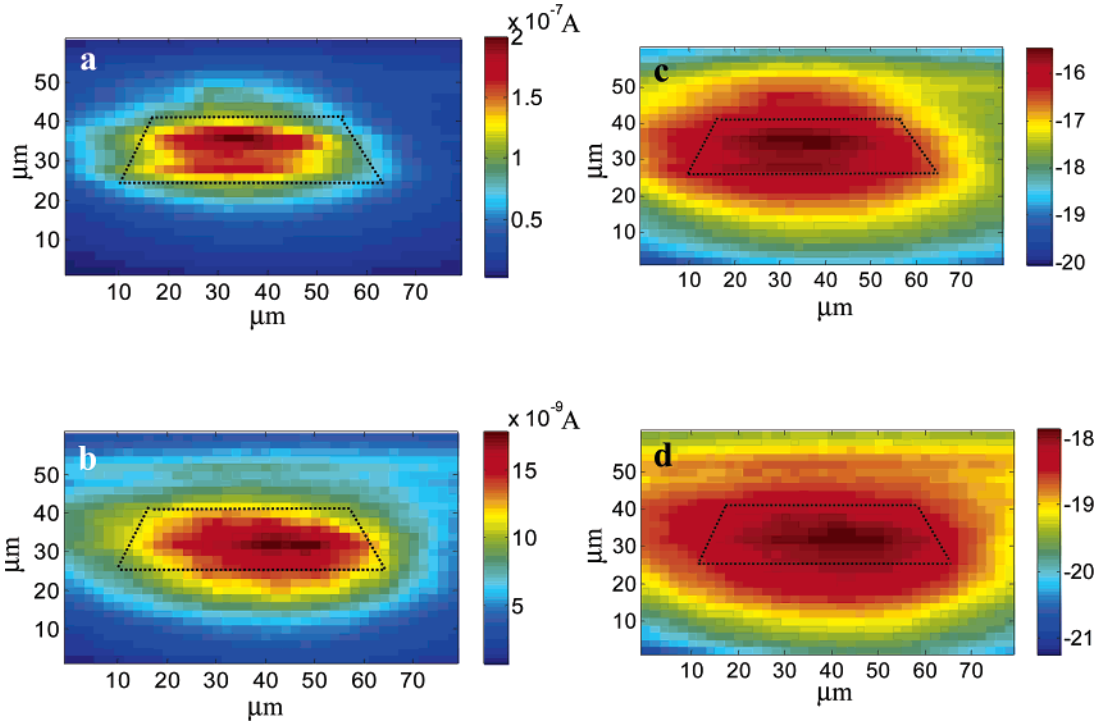

Figure 7. SECM images obtained at different electrode-to-channel distances in a PBS solution with a tip potential of −0.3 V and a separation HV of 1000 V. The electrode-to-channel distance was 12 μm for a and c and 17 μm for b and d. Images c and d were translated from images a and b, respectively, and are represented in ln *i*. Other conditions were the same as in Figure 2.

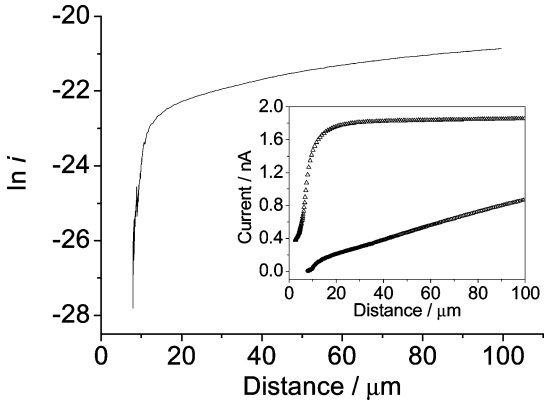

Figure 8. Dependence of ln *i* on the tip-to-channel distance. Data were measured in PBS solution at a detection potential of 1 V and a separation HV of 1000 V. Inset: current approach curve of Figure 8 (○) and the approach curve measured in the feedback mode of SECM (△). The curve shown in open triangles was obtained in PBS solution containing 1 mM $Ru(NH_3)_6Cl_3$ at a detection potential of −0.3 V without a separation voltage.

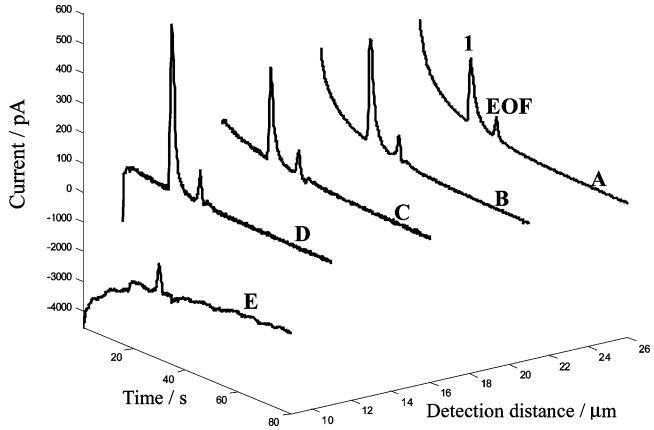

Figure 9. End-channel amperometric detection of dopamine at different detection distances. (A) 26 μm, (B) 21 μm, (C) 16 μm, (D) 11 μm, (E) 9 μm. Peak 1: dopamine; EOF: electroosmosis flow peak. Running buffer: PBS solution; separation HV: 1000 V; detection potential: 1 V; dopamine concentration: 0.2 mM.

normalized theoretical negative feedback curve to determine the tip-to-channel distance. On the basis of this calculated distance, the tip was withdrawn for a certain distance and then moved to the center of the channel and approached again. It could be seen that at larger tip-to-channel distances (e.g, ca. 100 μm) the separation HV had a negligible effect on the solution potential and the actual interfacial potential of the detection electrode. The observed anodic current corresponds to the electrooxidation of water. As the tip electrode approached the channel end, the tip current and ln *i* decreased monotonically over a relatively large distance ranging from 100 to 20 μm. This decrease reflects the fact that the solution potential along the central axial line increases slowly within the distance range mentioned above. In shorter tip-to-channel distances (<20 μm), the tip current and ln *i* decreased dramatically, which indicates a violent increase in solution potential. The increase in solution potential is due to the fact that the solution resistance decreases intensively and nonlinearly at the channel end. Therefore, the equipotential surfaces near the channel end are more intensive than those far from the channel. Further approach of the tip electrode to the channel end will lead to a dramatic conversion of the detection current from anodic to cathodic, which is caused by the enhanced coupling effect and the emergence of a separation current passing through the tip electrode (data not shown).

Following the results from Figure 8, the effect of solution potential on electrochemical detection was investigated at a tip-to-channel distance of around 15 μm. Taking dopamine as a model compound, separation parameters at different tip-to-channel distances were measured at a tip potential of 1 V. Figure 9 shows the electropherograms of neurotransmitter dopamine measured at detection distances ranging from 26 to 9 μm (curves A−E). The corresponding separation parameters are listed in

Table 1. Dependence of the Separation Parameters on the Electrode-to-Channel Distance[a]

electrode-to-channel distance (μm)	peak height (pA)	migration time (s)	half peak width (s)	peak skew[b]	separation efficiency (plates m^{-1})
11	516	19.8 ± 0.1	1.68	1.30	23 085
16	308	19.8 ± 0.1	1.70	1.41	22 545
21	312	20.0 ± 0.1	1.94	1.45	17 664
26	203	20.5 ± 0.1	2.08	1.48	16 145

[a] The data are the averages of five measurements. [b] Peak skew = (2 × area after apex)/(area before apex + area after apex).

Table 1. As the distance changed from 26 μm (curve A) to 11 μm (curve D), the starting background current decreased significantly, indicating a large decrease in the actual interfacial potential. As shown in Table 1, the migration time, half peak width, and peak skew also decreased with the decrease in detection distance. These parameters demonstrate that the convection and diffusion of the sample band also play important roles in the electrochemical detection in this region. At shorter detection distances, the sample band has less broadening and gives larger peak current. However, with the existence of the coupling effect and background noise, the change in peak current becomes more complex. In general, the peak current tends to increase at tip-to-channel distances ranging from 26 to 11 μm. This tendency shows that although the solution potential increases along with the decrease in the tip-to-channel distance, the actual tip potential is still high enough to oxidize dopamine. In this region, the convection and diffusion that mainly control the peak height. However, at a short detection distance of 9 μm (curve E), no oxidation current peak for dopamine is observed, and the baseline current changes from anodic to cathodic. This change in tip current demonstrates that the solution potential at this distance increases violently. This result is not surprising because Figures 7 and 8 have shown that at shorter tip-to-channel distances the interfacial potential of the tip electrode decreases violently along with the increase in the solution potential. Even for an applied tip potential of 1 V, the actual tip potential might decrease to a value where water/oxygen reduction occurs. It can also be seen that the peak current decreases a bit at a detection distance of 16 μm (curve C). This slightly inverted trend is considered to be caused by the synergistic effect of the increased solution potential, background noise, and limited convection and diffusion of the sample band. As we know, though the detection potential of 1 V is in the "plateau" part of dopamine oxidization, the decrease in the actual tip potential can also lead to a minor decrease in tip current. However, at this distance, the effect caused by limited convection and diffusion of the sample band is not large enough to compensate for this current loss. At a detection distance of 11 μm, the actual tip potential is still high enough to oxidize dopamine, and the reduced convection and diffusion promotes the regain of peak current.

It is worth noting that although the above method can precisely optimize the detection distance in a CE system, it is relatively time-consuming and expensive for this purpose. The coupling imaging method shall be used to probe the electric field distribution rather than the optimal electrode position. However, the tip radius is relatively large as compared to the dimension of the trapeziform channel, which prevents us from establishing a model to describe the relationship between the peak current and the separation field. For further research, the ratio of the tip radius (including the insulating layer) to the channel radius needs to be considered in calculating the tip current in the absence of an external electric field.

Conclusions

The newly developed SECM coupling imaging mode has been successfully used to map the distribution of the electric field at the end channel of CE microchips. The distribution of the electric field shows a dependence on the shape of the microchannel, separation HV, and tip-to-channel distance. The solution potential in the center of the microchannel is higher than that at the edge of the scanning plane, and the solution potential decreases with the increase in the detection distance. The coupling imaging mode of SECM has been proven to be powerful in investigating the properties of the electric field in solution. Future development of a theoretical description might be very helpful in the design of integrated amperometric detection systems in CE and the investigation of the potential distribution in biological membranes.

Acknowledgment. This work was supported by grants from the National Natural Science Foundation of China (NSFC, nos. 20299033, 20125515, and 20535010), the National Science Fund for Creative Research Groups (20521503), and the Hangzhou Cigarette Factory.

Supporting Information Available: SECM images measured at the end of a microchannel. This material is available free of charge via the Internet at http://pubs.acs.org.

LA0601049